Dexamethasone palmitate nanoparticles: An efficient treatment for rheumatoid arthritis

Mathilde Lorscheider, Nicolas Tsapis, Mujeeb Ur-Rehman, Françoise Gaudin, Ivana Stolfa, Sonia Abreu, Simona Mura, Pierre Chaminade, Marion Espéli, Elias Fattal

Dexamethasone palmitate nanoparticles: an efficient treatment for rheumatoid arthritis.

Mathilde Lorscheider[1], Nicolas Tsapis[1], Mujeeb ur Rehman[1,2], Françoise Gaudin[3], Ivana Stolfa[1], Sonia Abreu[4], Simona Mura[1], Pierre Chaminade[4], Marion Espeli[3], Elias Fattal[1]

[1] Institut Galien Paris-Sud, CNRS, Univ. Paris-Sud, Univ. Paris-Saclay, 92290 Châtenay-Malabry, France

[2]H.E.J. Research Institute of Chemistry, International Center for Chemical and Biological Sciences, University of Karachi, Karachi-75270, Pakistan.

[3] INSERM UMR 996, Univ. Paris-Sud, Univ Paris-Saclay, 92140 Clamart, France

[4] Lip(Sys)[2] EA7357, Lipides, systèmes analytiques et biologiques, Univ. Paris-Sud, Univ. Paris-Saclay, 92290 Châtenay-Malabry, France

Graphical Abstract

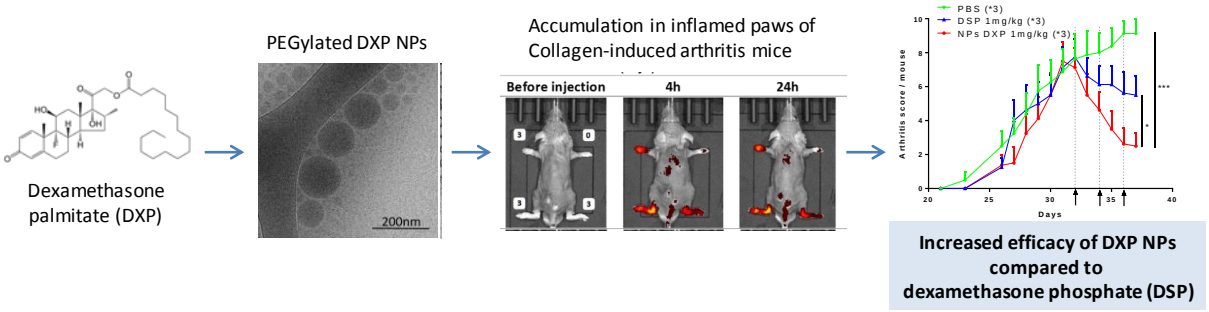

Abstract

Rheumatoid arthritis (RA) is a prevalent autoimmune disease characterized by joint inflammation, bone and cartilage erosion. The use of glucocorticoids in the treatment of RA is hampered by significant side effects induced by their unfavorable pharmacokinetics. Delivering glucocorticoids by means of nanotechnologies is promising but the encapsulation of highly crystalline and poorly water-soluble drugs results in poor loading and low stability. We report here the design of 130 nm nanoparticles made of solely dexamethasone palmitate, stabilized by polyethylene glycol-linked phospholipids displaying a negative zeta potential (-55mV), high entrapment efficiency and stability over 21 days under storage at 4°C. X ray diffraction showed no crystallization of the drug. When incubated in serum, nanoparticles released free dexamethasone which explains the *in vitro* anti-inflammatory effect on LPS-activated RAW 264.7 macrophages. Moreover, we demonstrate in a murine collagen-induced arthritis model the improved therapeutic efficacy of these nanoparticles. Their passive accumulation in arthritic joints leads to disease remission and recovery of the joint structure at a dose of 1mg/kg dexamethasone, without any adverse effects. Dexamethasone palmitate nanoparticles are promising in the treatment of inflammation in rheumatoid arthritis with a very significant difference occurring at the late stage of inflammation allowing to prevent the progression of the disease.

Keywords: nanomedicines; prodrug; glucocorticoid; arthritis.

1 Introduction

Rheumatoid arthritis (RA) is one of the most widespread chronic rheumatic diseases worldwide, with a prevalence of 0.5-1% in the developed countries [1]. RA is defined as a chronic, autoimmune rheumatic disease that affects all type of patients with a strong prevalence in 60-80 years old women and a female:male ratio of 3:1 [2]. RA evolves with inflammatory flares associated with inflammation of the joint synovial membrane, progressive bone and cartilage destruction and accompanied with strong pain [3]. Over the course of the disease, patients generally undergo a decreased quality of life, a potential disability and a reduction in life expectancy of about 10 years [4]. Like all autoimmune diseases, RA is caused by a disregulation of the immune tolerance leading to infiltration of the synovial membrane by immune cells (neutrophils, macrophages, T and B cells), pannus formation and proliferation of the lining cells of the synovial membrane [5]. Moreover, enhanced angiogenesis and high permeability of the newly generated vessels in a dense network all over the inflamed synovia, correlated with high vascular endothelial growth factor (VEGF) serum levels were reported in RA patients [6–8].

Within the RA therapeutic strategy, glucocorticoids (GCs) administration is limited to short period treatment to relieve joint inflammation during flares up due to their severe side effects [9]. GCs chronic administration for long-term treatment of RA, although not indicated, is used in association with first line treatment methotrexate or second line biologics by 1/3 of RA patients, preventing inflammation exacerbations. However, chronic misuse of GCs leads to the emergence of strong side effects such as diabetes, high blood pressure or Cushing syndrome [10,11]. Because of the ubiquitous expression of the GC receptor [12,13], GC local therapeutic activity is diluted by side activity in other organs. Therefore, patients require repeated administrations of high GCs doses strength to reach a sufficient anti-inflammatory activity in the tissue of interest [14].

Nanotechnologies are taking advantage of the specific physiopathology of inflamed tissues and of a vascular enhanced permeability effect to address encapsulated molecules to the tissue of interest by passive diffusion in diseased area [15,16]. Accumulation of therapeutic nanoparticles in inflamed joints could therefore improve anti-inflammatory activity while avoiding administration of high doses and thus reducing side effects [17].

Previous studies reported that in spite of their increased accumulation in pathologic areas, most of the nanocarriers used so far faced a very low GC drug loading, below 10%w/w [18–20], and a fast destabilization because of lipophilic GC crystallization in aqueous media impairing their efficacy. In the present study, we designed a new type of PEGylated nanocarrier made of dexamethasone palmitate (DXP). DXP is a prodrug of dexamethasone on which a palmitic chain is covalently linked by an ester bound. The presence of a C_{16} chain confers to the molecule a very high hydrophobicity and strong interactions with phospholipid aliphatic chains due to hydrophobic interactions [21–23]. These

PEGylated DXP nanoparticles (DXP-NPs), obtained by the sole addition of DSPE-PEG_{2000} as stabilizer, exhibit a high drug loading and stability over time. The collagen induced arthritis (CIA) mouse model was used to assess whether DXP-NPs display greater anti-inflammatory activity than free dexamethasone. Our results demonstrated that DXP-NPs lead to specific joint accumulation, strong reduction of joint inflammation and histopathological signs of arthritis without increased side effects.

2 Material and methods

2.1 DXP-NP preparation and physicochemical characterization

Nanoparticles were prepared by an emulsion-evaporation process. Briefly, 10ml of milliQ water were prechilled at 4°C. The desired amounts of DXP and DSPE-PEG_{2000}, respectively 50mg and 25mg, were dissolved in 1ml chloroform. The organic phase was injected into the water phase before pre-emulsification by vortexing for 30 seconds followed by ultrasonication during 2min at an amplitude of 40% in an ice bath (Branson, USA). The organic phase was evaporated under reduced pressure using a rotary evaporator. After full evaporation of the solvent, the suspension was stored at 4°C protected from light. Fluorescent nanoparticles were obtained by the same procedure, incorporating 4% (mol/mol DSPE-PEG_{2000}) of the hydrophobic and poorly-water soluble probe DID (1,1'-dioctadecyl-3,3,3',3'-tetramethylindodicarbocyanine, 4-chlorobenzenesulfonate salt) in the chloroformic phase. After each preparation, nanoparticles size (d_H), polydispersity index (PdI) and surface charge (zeta potential) were evaluated using a Malvern NanoZS at 173° angled laser (n=3 per sample, n=5 samples at least). Nanoparticle stability was followed up to 21 days while nanoparticles were stored in a cold room at 4°C. Size measurements were carried out in water and zeta potential at a 1/10 dilution in NaCl 1mM. Concentrations of DXP and DSPE-PEG_{2000} encapsulated were determined by HPLC-ELSD (evaporative light scattering detector) detection using a mobile phase of MeOH:ACN:Ammonium acetate (200mM, pH4) 70:28:2 added with 0.043% acetic acid and 0.104% trimethylamine, nebulization temperature of 35°C and evaporation temperature of 45°C, 30µl of samples were injected. DXP-NPs morphology was observed by TEM after negative staining with uranyl acetate at 2%(w/w) for 30 seconds and cryo-TEM images. Internal structure was examined by X-ray powder diffraction on the concentrated nanoparticle suspension (Supplementary information) compared to the crystalline form of dexamethasone obtained by recrystallization in acetone, using a Rigaku rotating copper anode automated diffractometer operating at 50kV and 200mA using Cu Kα radiation.

2.2 *In vitro* plasma release of Dexamethasone from DXP-NPs

DXP-NPs were diluted in water to yield a final equivalent concentration of dexamethasone (DXM) of 260 µg/mL. 180 µL of murine plasma were introduced in an Eppendorf tube and 20 µL of DXP-NPs were added and incubated at 37°C upon gentle mixing for different times up to 24h. After the

desired incubation time, 400 µL of acetonitrile containing 4µg/mL dexamethasone acetate as an internal standard was added followed by vortexing vigorously for 30 seconds to precipitate out enzymes/proteins present in plasma. Then, centrifugation was performed at 13, 400 rpm for 10 minutes (ST16R centrifuge, rotor TX-400, Thermo Scientific, France). The supernatant organic phase was collected and DXM was quantified by HPLC-UV as follows. A Waters 717 Plus autosampler chromatographic system was employed equipped with a Waters 1525 binary HPLC pump, a Waters 2487 dual λ absorbance detector, and a Breeze software. The analysis was performed at 240nm wavelength using a SymmetryShieldTM RP18 column (5 µm, 250×4.6 mm; Waters, Saint-Quentin-en-Yvelines, France). The column temperature was maintained at 40°C. The mobile phase was composed by a mixture of acetonitrile and milliQ water (35/65 v/v). The mobile phase flow rate was 1.2mL/min, the injection volume was 50µL and the run time was 30min. Retention times were 9min for DXM and 26min for dexamethasone acetate. Calibration curves of DXM were linear in the range 0.1-100µg/mL (R^2=0.9974, y=1.056x+0.1445).

2.3 In vitro anti-inflammatory effect

To verify that DXP-NPs were able to exert an anti-inflammatory effect equivalent to the free drug, RAW 264.7 cells were seeded in 24-well plates at a cellular density of $4x10^4$ cells/well in culture medium and were incubated for 48 hours until 80% confluency. Then, the medium was replaced by fresh medium alone or fresh medium with LPS at 0.1 µg/mL to induce inflammation, and plates were incubated another 3 hours. Afterwards, DXP-NPs were added at a subtoxic concentration [checked by the MTT (3-[4,5-dimethylthiazol-2-yl]-3,5-diphenyl tetrazolium bromide) colorimetric assay - unpublished data] diluted in culture medium: 100µg/mL of DXP and free dexamethasone phosphate (DSP) at 82µg/mL in culture medium, which correspond to 100µg/mL DXP considering molecular weight ratio. Culture medium alone was used as negative control and LPS 0.1 µg/mL as positive control. After 24 hours of incubation with the treatments, cell supernatants were collected and frozen at -20°C until analysis was performed. Cells were detached and counted. Mouse inflammatory cytokines TNFα and MCP-1 were quantified using a Cytometric Beads Array (CBA) detection kit (BD Biosciences, USA). In each test tube, 50µL of mouse inflammation capture bead suspension was added, completed with either 50µL of standards solution (20-5000pg/mL) or 50µL of supernatants samples. Phycoerythrin (PE) detection reagent was added 50µl to each tube and incubation during 2h at room temperature was performed. Samples were washed with 1mL wash buffer provided in the kit and tubes were centrifuged (200g, 5min) to recover the pellet. 300µL of wash buffer was added to resuspend the pellet and samples were quantified with the BD Accuri C6 Cytometer (BD Biosciences, USA). Cytokines results were analyzed with the FACP Array™ Software and were obtained as pg/mL concentrations. All measurements were performed in triplicate.

2.4 Animal studies

In vivo experimental procedures using DBA/1OlaHsd mice were approved by the ethical committee No 026 and by the French ministry of education and research (Accepted protocol No 2842-2015110914248481_v5). 9-12 weeks-old male DBA/1OlaHsd mice were purchased from Envigo (UK) and let for one week after shipping for adaptation before starting experiments. Mice were kept in a separate animal room under climate-controlled conditions with a 12h light/dark cycle, housed in polystyrene cages containing wood shavings and fed with standard rodent chow and water *ad libitum*.

2.4.1 Collagen induced arthritis mice model

At day 0, 10-13 weeks-old male DBA/1OlaHsd mice were injected intradermally at the base of the tail with an emulsion of Complete Freund's Adjuvant (CFA) and type II collagen (CII). At day 21, mice received a boost injection of the same composition. From day 21, mice were evaluated every 2 days during the first week after boost and every day from day 28. Weight and arthritis symptoms were monitored, based on a visual scoring scale (0-3) of the paws with evaluation of the erythema, swelling and ankylosis of each paw (Fig. S3) and hind paw volume was measured with a plethysmometer (Harvard Apparatus). Special care was paid to ensure sufficient food and water access to mice.

2.4.2 Assessment of the therapeutic efficacy in mice

CIA mice were divided in 5 groups (n=8) on day 31 based on the inflammation score and hind paw volume to create the most homogeneous groups in terms of inflammation. On days 32, 34 and 36, mice received intravenously PBS or free dexamethasone sodium phosphate at 0.1 mg/kg (*eq.DXM*) or 1mg/kg (*eq.DXM*) or DXP-NPs at 0.1 mg/kg (*eq.DXM*) or 1mg/kg (*eq.DXM*). From day 21 to 37, arthritis was monitored as described above. Mice were sacrificed on day 37, paws were removed for histology experiments.

2.4.3 DXP-NPs joints accumulation

Healthy (n=4) and CIA mice (n=4 at least, at day 32 post CIA induction) were injected intravenously with (i) fluorescent DXP-NPs-DID4% at 1mg/kg (*eq. DXM*) or (ii) a solution of free DID in DMSO/glucose5% 1/9 v/v (i.e. control). DXP-NPs and free dye-treated mice received comparable amounts of DID (0.1mg DID/kg). The kinetics of nanoparticles and free DID biodistribution were evaluated by NIR *in vivo* imaging using the IVIS Lumina® LT Series III (PerkinElmer, USA). After excitation at 640nm the signal was recovered at 745nm emission filter. First fluorescence images

were recorded at t=4h post injection and then mice were imaged daily until the disappearance of the fluorescent signal (day=14). Images of each mice before treatment were used to determine the baseline level of fluorescence (i.e., auto-fluorescence) which was subtracted to the recorded signal. Mice were imaged both in ventral and dorsal position. Images were processed using the Living Image software (PerkinElmer, USA). A region of interest was automatically identified, and quantification was performed using the Average radiant efficiency value (threshold of 30%). Results are expressed as [fluorescence signal on the analyzed surface subtracted by the auto-fluorescence acquired before injection] as a function of the inflammation score of each paw.

2.4.4 Histopathology studies

After sacrifice of the mice, hind legs were removed on day 37 from CIA mice at the end of the efficacy study. Skin and muscles were removed, and hind legs (from above the knee to the end of the foot) were fixed 24h in 4% paraformaldehyde and decalcified for 8h in Microdec (Microm Microtech, France). Hind legs were included in paraffin blocks and sectioned in 4µm thick slides. Haematoxylin-eosin-safran *(*HES) staining was performed and synovial cell infiltration, pannus formation and proliferation and bone erosion were individually scored on a 0-3 scale as follows [20,24]. The score for every histopathologic feature was summed for each animal.

Synovial infiltration. 0: normal; 1: minimal infiltration of cells in synovium and synovial membrane; 2: mild infiltration with minimal synovial hyperplasia; 3: severe infiltration in synovium and periarticular tissue.

Pannus. 0: normal; 1: minimal pannus formation, marginal zones; 2: mild cell proliferation and expansion; 3: severe infiltration with large pannus expansion.

Bone and cartilage erosion: 0: normal; 1: slight erosion, bone and cartilage thickness reduced; 2: mild bone and cartilage structure modification, thin bone and cartilage thickness; 3: severe erosion, total destruction of joint architecture.

2.5 Adverse effect evaluation

CIA was induced on 30 DBA/1 mice as described in the dedicated section above. On day 31, mice were divided into 3 groups (n=10), based on the inflammation score and hind paw volume to create the most homogeneous groups in terms of inflammation. After 3 IV injections on days 32, 34 and 36 with PBS or DSP 1mg/kg (*eq.DXM*) or DXP-NPs 1mg/kg (*eq.DXM*), CIA mice were sacrificed on day 37. Blood was recovered by intracardiac puncture, one part of total blood was dedicated to complete blood count (CBC) and the other was centrifuged to recover plasma. Quantification of plasmatic glucose, alanine-aminotransferase (ALAT), aspartate-aminotransferase (ASAT) and creatinin; and

complete blood count (CBC) from total blood were performed by Cerbavet (France). Standard values presented on graphs correspond to mice standard values, without distinction between strains.

2.6 Statistical analysis

Results were reported as mean ± standard error of the mean (SEM). Statistical analysis was performed using the GraphPad Prism 6.0 software.

3 Results and discussion

3.1 DXP-NPs preparation and characterization

DXP-NP formulation process is based on the emulsion-evaporation method (Fig. S1). Briefly, DXP and DSPE-PEG_{2000} were dissolved in chloroform and injected in pre-chilled aqueous phase. Emulsion was obtained through vortexing and sonication steps followed by chloroform evaporation leading to the formation of nanoparticles. DXP alone did not form nanoparticles. However, in combination with DSPE-PEG_{2000}, recognized as biocompatible and approved by the Food and Drug Administration for medical use [25], and due to hydrophobic interactions between the palmitic chain of DXP and stearic chains of the PEGylated lipid [26], the emulsion-evaporation method led to the formation of spherical nanoparticles. The obtained nanoparticles presented a hydrodynamic diameter (d_H) of 130nm and a negative surface charge of -55mV (Fig. 1a), contributing to the stability and preventing nanoparticle aggregation upon storage. The polydispersity index (PdI) of 0.2 confirmed a monodisperse population of DXP-NPs, correlated to transmission electron microscopy (TEM) pictures also showing the spherical structure of DXP-NPs (Fig. 1c). The poor water solubility of DXP usually induces its crystallization in the nanoparticle suspension [26], leading to a low drug loading [18] and destabilization of the suspension overtime. The presence of DSPE-PEG_{2000} clearly avoided the formation of prodrug crystals and DXP-NPs with an amorphous structure were obtained. Indeed, no diffraction peaks were observed by X-ray diffraction for DXP-NPs, however a bump characteristic of an amorphous organization was detected. On the contrary, DXP crystals exhibited many diffraction peaks as expected [22,26]. Cryo-TEM images (Fig. 1b and 1c) confirmed the amorphous structure as no crystals were observed. In addition, DXP-NPs presented a very high DXP encapsulation efficiency of 98%w/w corresponding to a prodrug loading of 78%w/w and a drug loading of active dexamethasone (DXM) of 48.9%w/w. Compared to previous literature, our approach thus led to a much-improved loading efficiency. For example, the DXP-loaded lipid emulsion currently marketed in Japan and in Germany under the trademark Limethason® or Lipotalon® for the treatment of chronic inflammatory pathologies incorporates only 4%w/w of DXP/lipids [27]. Moreover, the encapsulation of DXP within solid lipid nanoparticles (SLN) by Kim at al. [28] leads to a DXP loading of 4-25%w/w lipids, in line with the 2.2 and 6.6%w/w lipids incorporation rate obtained by Lu and al. [29] . The high

drug loading of DXP-NPs could facilitate the administration of efficient therapeutic doses with low excipients amounts. In the DXP-NPs, 53% of initial DSPE-PEG_{2000} was encapsulated in DXP-NPs, the remaining being present in the formulation as micelles along with DXP-NPs suspension. DXP-NPs stability was assessed over 21 days under storage at 4°C and presented an excellent profile with no modification of size, polydispersity, surface charge or internal structure as assessed by X-ray diffraction (Fig. 1b and 1d). The good stability most probably arises from the presence of encapsulated DSPE-PEG_{2000}. PEG chains exposed at DXP-NPs surface confer stability by steric repulsions whereas stearic chains associated to palmitic chains of DXP by hydrophobic interactions prevented DXP crystallization. PEGylated DXP-NPs were obtained without any addition of surfactants or stabilizers that could reveal toxic after administration, such as chitosan, poloxamer or PVA [30]. This simple preparation process with low amounts of PEGylated lipids presents obvious advantages from a toxicological point of view over common solid lipid nanoparticle formulations and from a formulation point of view with an increased drug loading and DXP stability. PEGylated DXP-NPs were incubated and the release of free DXM was monitored by an HPLC method (Fig 1e). The release profile shows that about 60% of dexamethasone is released before reaching a plateau more likely due hydrolysis through esterases present in plasma. The reason for which DXM is partly unreleased is unclear but might result from partial degradation of dexamethasone.

a

DXP-NPs	
d_H (nm)	130 ±3
PdI	0.2
Zeta-potential (mV)	-55 ±2
DXP encapsulation efficiency (%)	98.8 ±0.6
DXM loading (%w/w)	48.9 ±0.6
DSPE-PEG_{2000} encapsulation efficiency (%)	53.1 ±7.7

b

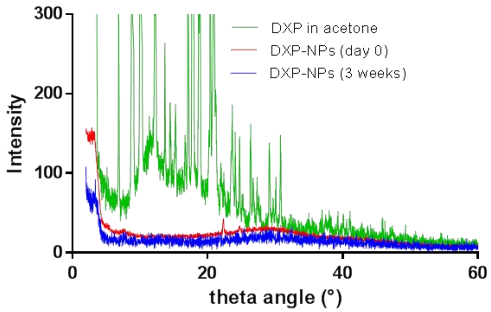

c

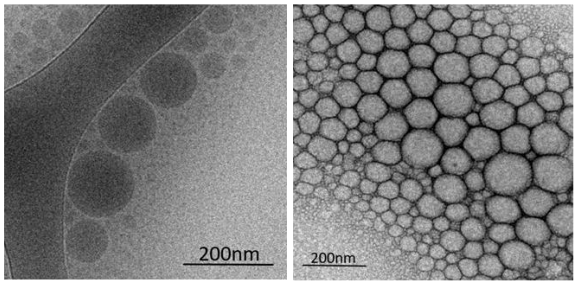

d

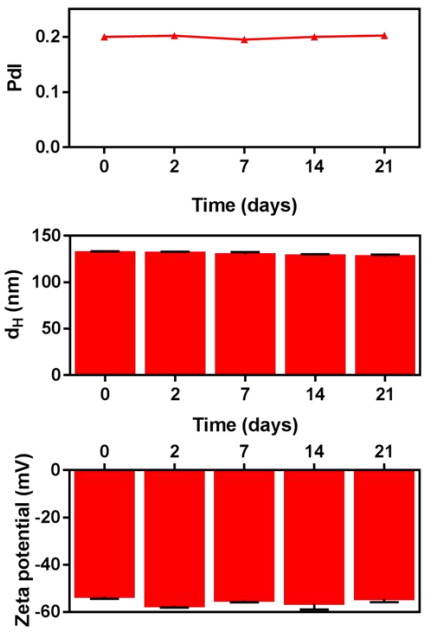

e

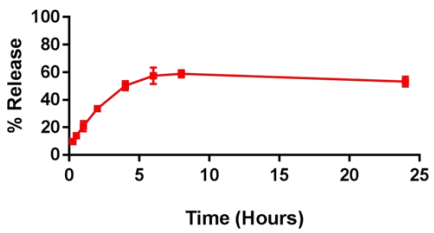

Fig. 1: Characterization and stability of DXP-NPs. **a.** Main physico-chemical parameters of DXP-NPs. Nanoparticles exhibited a monodisperse population of 130nm with negative surface charge and high drug loading of 49%w/w (eq. DXM/particle) **b.** X-ray diffractogram of DXP crystals (green) presented several diffraction peaks characteristics of a crystalline structure. By contrast, no peaks were observed for DXP-NPs either the day of preparation (red) or after 3 weeks of storage at 4°C (blue). **c.** Cryo-TEM (left) and TEM (right) images confirmed size measurements and the amorphous structure of DXP-NPs. **d.** DXP-NPs size, zeta potential and polydispersity index (PdI) stability at 4°C were followed up to 21 days. Results are presented as mean ± SEM (n=5 samples at least, each sample was analyzed in triplicate). **e.** In vitro release in plasma of dexamethasone from DXP-NPs.

3.2 *In vitro* anti-inflammatory effect

To ensure that the anti-inflammatory activity of DXM was conserved after formulation, the release of the pro-inflammatory cytokines MCP-1 and TNFα by LPS-activated macrophages into the cell culture medium was quantified after their exposition to DXP-NPs at the concentration of 100µg/mL DXP or free DSP at 82µg/mL, corresponding to 100µg/mL of DXP. A decrease of cytokines concentration was clearly observed resulting from the anti-inflammatory effect of DXP-NPs (Fig. 2). The MCP-1 chemokine (Fig. 2) was strongly and significantly reduced by DXP-NPs in presence of LPS. The same conclusions hold for the secretion of TNFα (Fig. 2). These results demonstrate the maintenance of a similar anti-inflammatory activity between free drug and the drug released from the DXP-NPs.

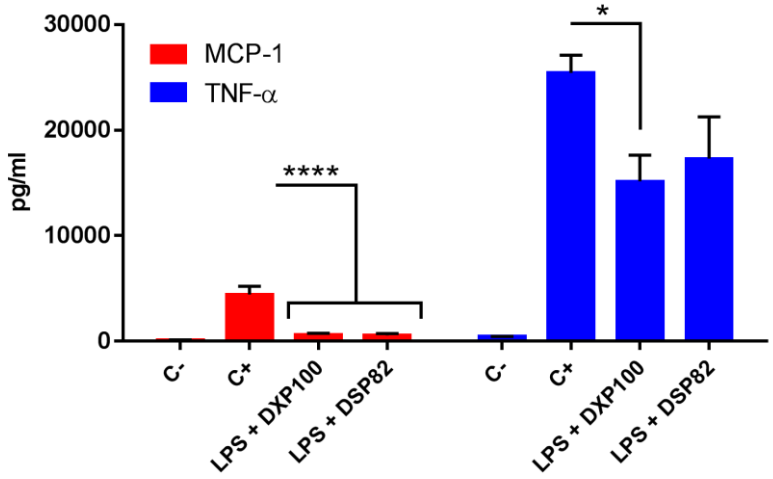

Fig 2: Cytokine production by Raw 264.7 macrophages without LPS induction (C-) or with LPS induction 0.1µg/mL (C+), DXP nanoparticles at 100µg/mL (LPS+DXP100) or DSP solution at 82µg/mL corresponding to 100µg/mL of DXP (LPS+DSP82). MCP-1 and TNF-α. Results are presented as mean±SEM (n=3) for all groups. Statistical analysis was performed with two-way ANOVA followed by Tukey's post test. * p<0.05, **p<0.01, ***p<0.001, ****p<0.0001 indicates differences with positive control (C+).

3.3 *In vivo* activity on rheumatoid arthritis and inflamed joint accumulation

To assess DXP-NP efficacy on rheumatoid arthritis, a collagen-induced arthritis (CIA) model was developed on DBA/1 male mice [31]. The effect of DXP-NPs on paw arthritis inflammation score and volume of hind paw edemas was compared to free dexamethasone sodium phosphate (DSP) and PBS

as negative control (Fig. 3). A low dosage, 0.1mg/kg *(eq.DXM)*, injected intravenously three times every two days was compared to a medium dosage at 1mg/kg *(eq.DXM)*, with the same injection pattern. These doses were considered since the administration of 1mg/kg *(eq.DXM)* is widely used in the literature as a medium dose to treat animals in arthritis mouse models without induction of side effects [32]. Before the first injection (day 31), mice were randomly divided into 5 groups with the same average total arthritis score of 7.5 per mouse. The first injection took place at day 32 after the induction of CIA, a time point corresponding to the peak of the disease (Fig. S3). The activity of DXP-NPs 0.1mg/kg *(eq.DXM)* was evaluated by measuring the total arthritis score on all 4 paws for each mouse and showed no significant reduction of the inflammation compared to free drug or PBS after statistical analysis on the whole length of the experiment. Indeed, the arthritis score on day 37 of DSP 0.1mg/kg (*eq.DXM*) group was 6.1±1.4 whereas the equivalent dose of DXP-NPs exhibited an arthritis score of 7.7±1. However, a significant difference was observed on hind paw volumes between DXP-NPs at 0.1mg/kg *(eq.DXM)* (0.15±0.006ml), free drug at 0.1mg/kg *(eq.DXM)* (0.18±0.01ml) and PBS (0.2±0.01ml) on day 34 (Fig. 3c). The discrepancy between the two evaluation methods may arise from the fact that arthritis score measurement is based on several parameters such as paw edema, swelling, redness and the number of affected fingers (Fig. S3), whereas hind paw volume measurement is only based on the edema evaluation. Moreover, arthritis score is measured on all 4 paws whereas paw volumes is measured only on hind paws. Thereby a slight reduction of edema will immediately affect the paw volume but not the total arthritis score. Strikingly, a medium dose of 1mg/kg *(eq.DXM)* of DXP-NPs showed a strong activity on disease progression with a significant reduction of the arthritis score compared to free dexamethasone (DSP) at the same dose and to the control group (PBS). After three injections of DXP-NPs 1mg/kg *(eq.DXM)*, the total arthritis score dropped down to 2.5±0.7, significantly differing from what we observed for the groups DSP 1mg/kg *(eq.DXM)* (5.5±1.1) and PBS (9.1±0.8) at day 37. The analysis of hind paw volume on day 34 and up to ay 37 (Fig. 3c and 3b) confirmed the strongest therapeutic efficacy of DXP-NPs (0.14±0.003ml) *(eq.DXM)* with significant reduction compared to the free drug DSP at 1mg/kg (0.15±0.006ml) and the PBS group (0.2±0.01ml). By analyzing hind paw volumes, we can also conclude that treatment with DXP-NPs 0.1mg/kg *(eq.DXM)* exhibited the same anti-inflammatory activity at day 34 (0.15±0.006ml) than DSP 1mg/kg *(eq.DXM)* (0.15±0.006ml). Therefore, a reduction of the administrated dexamethasone doses through replacement of free drug by DXP-NPs could be considered. Numerous studies reported the accumulation of nanoparticles in inflamed sites [20,33] associated with an increased number of vessels in synovium induced by the high VEGF serum concentration [34]. Angiogenesis is correlated to clinical arthritis score and new vessels present high endothelial permeability to allow diapedesis of activated macrophages and lymphocytes leading to synovial infiltration [6,35]. Thereby, long-circulating nanoparticles may passively diffuse through

endothelial pores and specifically accumulate in inflamed joints due to extravasation and further macrophage uptake [36]. DXP-NPs with stealth properties due to the presence of PEG at their surface could circulate longer in blood vessels and produce a rapid, significant anti-inflammatory activity on inflamed joints, leading to a complete remission of rheumatoid and persistent arthritis observed after treatment with 1mg/kg *(eq.DXM)* DXP-NPs. Indeed, as shown by preliminary biodistribution studies, the stealth effect favors a lower uptake by the liver compared to the free drug (Fig. S7). The mechanism by which such nanoparticles exert their anti-inflammatory effect is not totally clear. Nanoparticles might be taken up intact by synovial lining macrophages (more likely M1) as described [37], however we cannot rule out the possibility that the nanoparticles are degraded at the extracellular level, releasing free DXM that enter freely into macrophages without any specificity.

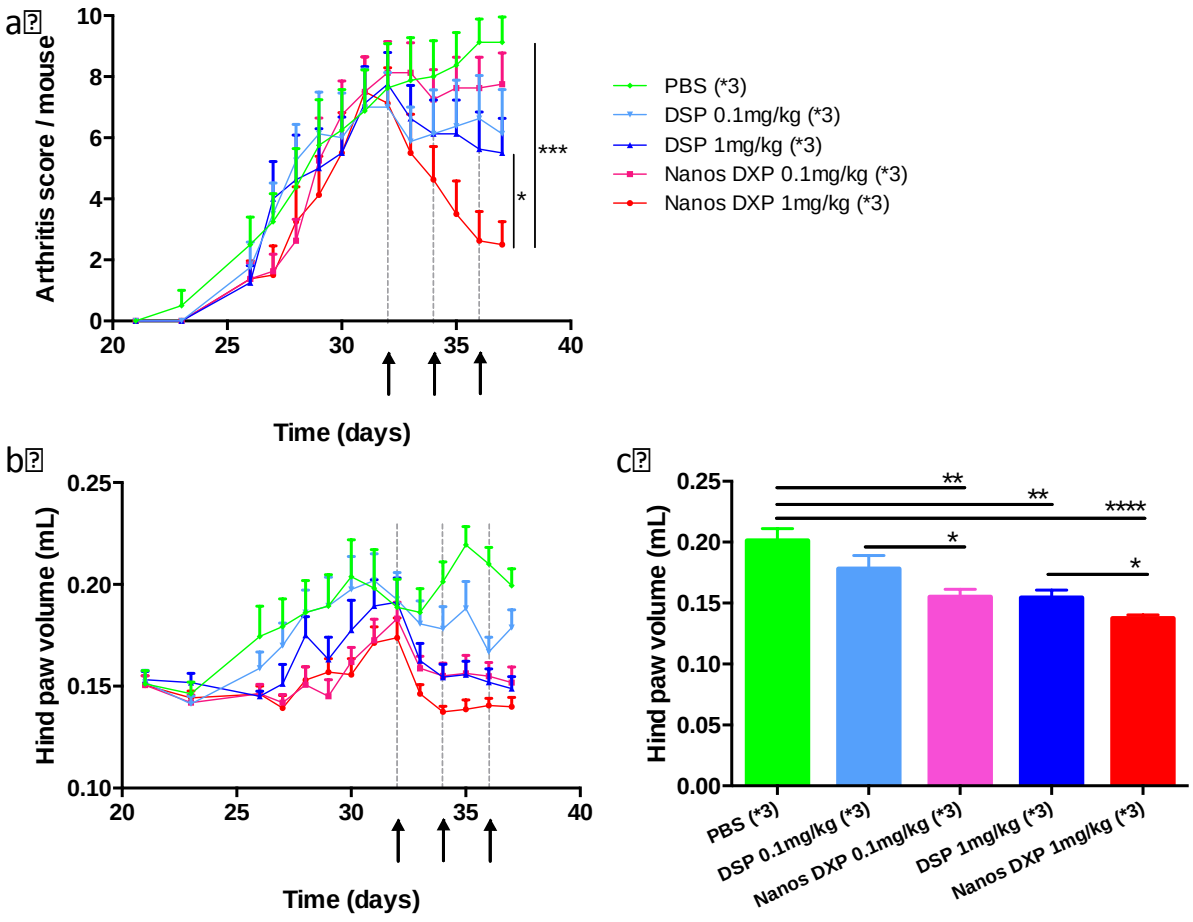

Fig. 3. Therapeutic activity of DXP-NPs on a collagen induced arthritis (CIA) mouse model. 31 days after CIA induction, mice were divided into 5 groups (n=8) presenting similar arthritis score (7.5 average arthritis score). Each group received three intravenous injections of treatments or controls on days 32, 34 and 36. **a.** Arthritis score and **b**. hind paw volume. The negative control group received PBS (green diamonds), free drug groups received dexamethasone sodium phosphate (DSP) at 0.1mg/kg (eq.DXM) (light blue triangles) or 1mg/kg (eq.DXM) (dark blue triangles), DXP-NPs were administered at 0.1mg/kg (eq.DXM) (pink squares) or 1mg/kg (eq.DXM) (red circles). After three IV injections, DXP-NPs 1mg/kg (eq.DXM) induced a significant reduction on arthritis score compared to DSP at the same dose and to PBS. Statistical analysis was performed with two-way ANOVA and Newman-Keuls post-test (*p<0.05, ***p<0.001). **c.** Hind paw volume measured on day 34. The

volume of DXP-NPs 0.1mg/kg (eq.DXM) group (pink) was significantly different from free drug 0.1mg/kg (eq.DXM) (light blue) and from PBS group, proving the superior efficacy of DXP-NPs. At a higher dose of 1mg/kg (eq.DXM), DXP-NPs (red) group presented a significantly lower hind paw volume than DSP (dark blue) and PBS. Statistical analysis was performed with Mann-Withney test (*p<0.05, **p<0.01, ****p<0.0001).

To confirm the hypothesis of accumulation of stealth DXP-NPs in inflamed joints, fluorescent nanoparticles were formulated to monitor the *in vivo* distribution of DXP-NPs after IV administration. DID (1,1'-dioctadecyl-3,3,3',3'-tetramethylindodicarbocyanine, 4-chlorobenzenesulfonate salt) (Fig. S2a), a lipophilic fluorescent label containing two aliphatic chains was introduced in the organic phase before emulsification (4%mol with respect to the DSPE-PEG_{2000}). No significant differences in terms of size and PdI were observed between fluorescent NPs and non-fluorescent ones (Fig. S2b). CIA and healthy mice received a single intravenous injection of fluorescent DXP-NPs-DID4% at a dose of 1mg/kg *(eq.DXM)*. Day 32 post-disease induction was selected for the treatment as it corresponded to the peak of the inflammation. Due to the heterogeneity of joint inflammation inherent to the CIA model not all paws of all injected mice were affected, and we took advantage of this to assess DXP-NP accumulation in inflamed vs. non-inflamed paws from the same animal. After injection of the fluorescent NPs, near infrared (NIR) images of mice were recorded non-invasively for up to 14 days, and the fluorescence signal on the 4 paws of each mouse was quantified. At 4h post NP injection, a slight increase of fluorescence signal was observed in the paws of healthy mice, which corresponded to the presence of nanoparticles in the vasculature. However, the signal, reached the baseline value (mouse auto-fluorescence) at 24h, without further modification until the end of the study (Fig. 4a and 4c). Among four CIA-treated mice, an intense fluorescent signal was measured in the paws of mice, which displayed a severe paw inflammation (arthritis score = 3). This signal peaked at 24 hours post-injection and then progressively decreased to baseline value by day 14 (Fig. 4a and 4c). As expected, in absence of inflammation, (arthritis score = 0) the fluorescence signal in the in the paws of CIA mice overlapped that recorded after injection of NPs in healthy mice, thus clearly revealing that joint accumulation of DXP-NPs was dependent on edema and neovascularization. An intermediary level of fluorescence intensity was recorded in the paws displaying an arthritis score between 1 and 2 (pooled results for a better statistical analysis), thus demonstrating the impact of inflammation stage on neoangiogenesis and therefore on DXP-NPs accumulation. Of note, the same profile was observed both on ventral and dorsal images (Fig. 4b and Fig. S4). Fig. 4b presents the average radiant efficiency (fluorescent signal) at 24h after injection on dorsal images with a significant difference between strongly inflamed paws (arthritis score = 3) and slightly (arthritis scores = 1 and 2) or not inflamed paws (arthritis score = 0 and healthy). The same trend was obtained when ventral pictures were analyzed (Fig. S4).

As a control, a DID solution containing the same amount of probe than DXP-NPs-DID4% was also injected to CIA and healthy mice (Fig. S5). The fluorescence signal detected was slightly correlated to the inflammation score due to the high vessel density in inflamed joints. However, the fluorescence intensity was significantly higher (1.5 to 2 times higher) on inflamed paws after DXP-NPs-DID4% administration compared to free DID solution, supporting that joint accumulation is linked to DXP-NPs diffusion and not to an inherent DID property. These results clearly confirm the accumulation and cellular uptake of nanoparticles in the inflamed joints 5 times higher than in non-affected joints. This accumulation and retention further explain the improved therapeutic efficacy of DXP-NPs compared to the free soluble DSP, which does not accumulate specifically in inflamed joints. Whether this accumulation is due to macrophage uptake in the synovial fluids very likely as suggested by several authors [37,38]. Another possibility would be that nanoparticles are taken up by monocytes that are then being used as carriers to the inflammation site. Particle are then cleared from the paws as demonstrated by a slow and progressive reduction of fluorescence that occurred after 24 hours. This decrease of fluorescence might be related to particle degradation at the site of action and further elimination of the probe.

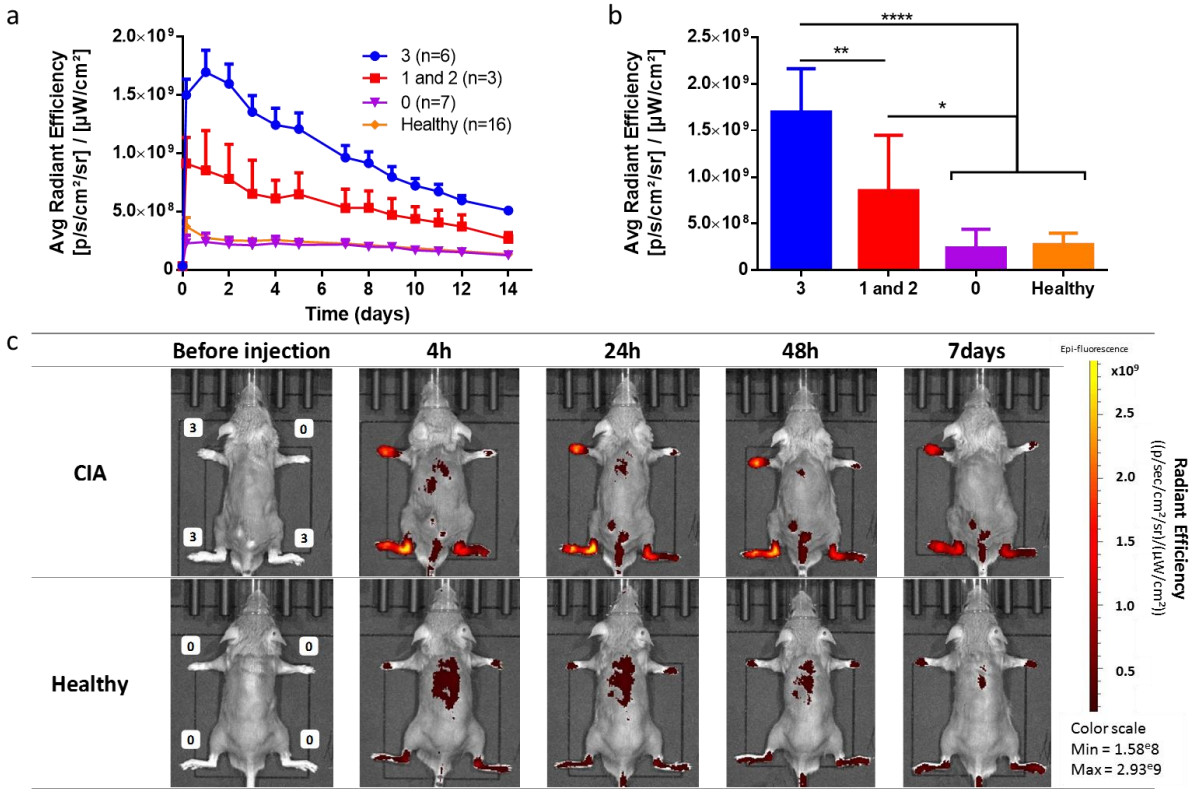

Fig. 4. Accumulation of DXP-NPs in inflamed joints, impact of arthritis severity. After IV injection of fluorescent nanoparticles, the evolution of the NIR signal (dorsal view) in healthy mice (n=4) and CIA mice (n=4) was monitored according to the arthritis score for each paw. **a.** Fluorescent signal in paws segregated on the basis of their arthritis score after IV injection with DXP-NP-DID4% for 14 days. Paws of healthy mice (yellow diamonds) and score 0 paws of CIA mice (purple triangles) displayed the same basal level of fluorescence, score 1 and 2 paws of CIA mice presented an increase in

fluorescence signal above the auto-fluorescence level up to 48h after injection followed by a slow decrease down to basal level after 14 days. Highly inflamed paws (score 3, blue dots) displayed a strong fluorescence signal with a maximal level 24h after injection. **b.** Fluorescent signal in paws segregated based on their arthritis score 24h after IV injection with DXP-NP-DID4%. Nanoparticles accumulation in highly inflamed paws (score 3, blue) was significantly higher than mildly inflamed paws (score 1 and 2, red) and regular paws (score 0, purple/ healthy, yellow). The strongest joint inflammation, the highest nanoparticles accumulation. Statistical analysis was performed with one-way ANOVA and Tukey post-test (*p<0.05, **p<0.01, ****p<0.0001). **c.** In vivo representative images of one mouse per group before and after injection with DXP-NP-DID4% at 4 hours, 24 hours, 48 hours and 7 days. The score of each paw is indicated in white squares on the "before injection" image.

3.4 Histological evaluation of formulation efficacy

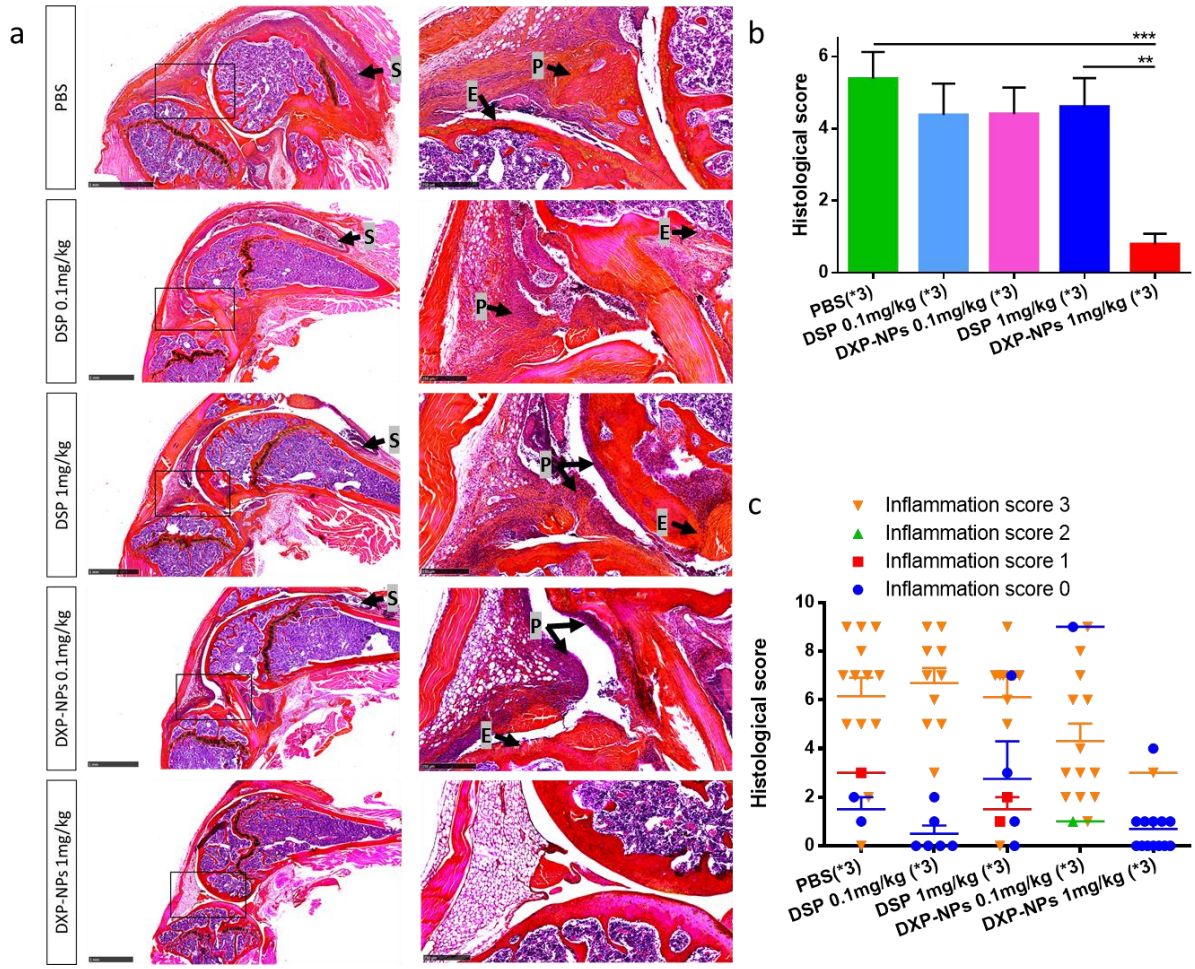

Fig. 5. Histopathological evaluation of the knee joint inflammation after DXP-NPs treatment. a. Haematoxylin-eosin-safran (HES) staining of one representative knee joint section for each group of treatment: PBS, DSP 0.1mg/kg (eq.DXM) and 1mg/kg (eq.DXM), DXP-NPs 0.1mg/kg (eq.DXM) and 1mg/kg (eq.DXM). For each slide, the synovial infiltration (S), the cell proliferation inside the synovial membrane forming the pannus (P) and the bone and cartilage erosion (E) were visually scored from 0 to 3 giving a maximal histological score of 9 per slide. **b.** The average histological score for each treatment group is shown. **c.** Relation between the histological score and the macroscopic visual inflammation score observed on day 37 for each group of treatment. n=8 mice per treatment group, right and left knees for each mouse were evaluated. Statistical analysis was performed with one-way ANOVA and Tukey post-test (*p<0.05, **p<0.01, ****p<0.0001)

To confirm the therapeutic efficacy of DXP-NPs observed on a macroscopic scale (Fig. 2), histological structures of knees were evaluated. After treatment with three IV injections (days 32, 34, 36) of PBS, DSP 0.1mg/kg (*eq.DXM*) and 1mg/kg (*eq.DXM*) or DXP-NPs 0.1mg/kg (*eq.DXM*) and 1mg/kg (*eq.DXM*), mice were sacrificed on day 37 post collagen injection and knee joints were observed and inflammation was scored after HES staining. As expected, the control group injected with PBS presented a high level of inflammation with pannus formation associated with an important synovial infiltration, a synovial lining cell proliferation and strong bone erosion. DSP treatment at both doses did not demonstrate a significant impact on the knee histopathology compared to the PBS control group. Although not statistically significant, the administration of DXP-NPs at 0.1mg/kg (*eq.DXM*) tended to decrease the histological severity of the inflammation. In striking contrast, the medium dose of DXP-NPs 1mg/kg (*eq.DXM*) led to a significant reduction of inflammatory histological signs compared to the same dose of DSP and to PBS. A good correlation between the histological scores and the macroscopic arthritis scores determined on each paw before sacrifice was obtained confirming the soundness of our first analysis (Fig. 4c). In the DXP-NPs 1mg/kg (*eq.DXM*) treatment group, a very few number of knee joints presented mild synovial hyperplasia with cell proliferation and fibrosis. These histological results are in agreement with therapeutic efficacy and joint accumulation results described above. Therefore, the benefit of three IV injections of DXP-NPs 1mg/kg (*eq.DXM*) was clearly demonstrated compared to the free DSP at the same dose.

3.5 Effect of formulation on glucocorticoids side effects

Chronic administration of high doses of GCs generally leads to appearance of strong side effects such as hepatic and renal impairment, diabetes or hematologic abnormalities [3,37–39], which therefore, limit their use in chronic auto-immune diseases such as RA. DXP-NPs proved their superior therapeutic efficacy in our CIA mouse model after three IV injections of a medium dose of 1mg/kg (*eq. DXM*) compared to DSP (Fig. 3a). Adverse event assessment was designed to compare DXP-NPs to DSP, currently considered as the standard IV treatment, at the same therapeutic dose of 1mg/kg (*eq.DXM*) and PBS as negative control, 24h after the last IV injection. Hepatic enzymes were quantified to evaluate liver function. Alanine aminotransferase (ALAT) plasmatic concentration (Fig. 6a) did not present significant increase between groups. Asparagine aminotransferase (ASAT) (Fig. S6) showed a very slight increase for the DXP-NPs treatment group compared to PBS but no difference was observed with DSP. DSP and DXP-NPs exhibited a similar and moderate increase of creatinin plasmatic concentration and blood glucose concentration (Fig. 6b and 6c) compared to control (PBS) but no difference between both treatment groups was detected, indicating no damage of liver, pancreas, or kidneys after DXP-NPs administration. The fact that there is no difference between treatment in relation with markers in line with liver function (glucose, liver enzymes) might

results from liver biodistribution observations. Indeed, although DXP-NPs and DXM display different level of liver distribution (lower than 5% and higher than 15% of the injected dose, respectively) (Fig. S7), DXM resulting from the prodrug hydrolysis induces an equivalent liver distribution (around 12%) (Fig. S7) both just enough to induce hyperglycemia or slight liver enzymes increase.

During the progression of the disease, the mice weight was monitored and no significant difference between groups in terms of weight loss were observed. All groups lost weight due to the strong impact of CIA inflammation, but DSP 1mg/kg (*eq.DXM*) treated group seems to undergo a greater weight loss with a maximum of -13% of their initial healthy weight. Hematological parameters (blood count and leukocytic formula) were evaluated on total blood samples after sacrifice on day 37. No modification of blood count was observed for DXP-NPs as well as for DSP compared to PBS group. Hemoglobin concentration (Fig. 6e) and mean corpuscular volume (MCV) (Fig. 6f) were not affected by any treatment either. Mice did not present anemia, red blood cell count was slightly increased compared to standard values, hematocrit, mean corpuscular haemoglobin (MCH) and mean corpuscular haemoglobin concentration (MCHC) were comprised within standard values (SI Fig. 6) showing no hematological adverse effects of DXP-NPs 1mg/kg (*eq.DXM*). White blood cell count (Fig. 6g) was similar between the DXP-NPs and DSP groups although they both exhibited higher values compared to the PBS control group. This leukocytosis is linked to neutrophilia and basophilia (Fig. S6) that are exacerbated in the GC treated groups. This pattern of leukocytosis is described as the typical response 24h after GC exposure [37]. Lymphocyte count was also slightly increased in the DSP and DXP-NP groups compared to the PBS group, but values remained within the range of standard values (Fig. 5h). No modification of eosinophils, monocytes and platelets was observed (Fig. S6).

These results confirmed that only mild adverse effects were observed after 3 IV injections of DXP-NPs 1mg/kg (*eq.DXM*). Moreover, these adverse effects were not significantly different from those observed after 3 IV injections of DSP at the same dose. Furthermore, it is important to note that DSP 1mg/kg (*eq.DXM*) do not induce such a drastic reduction of the inflammation as observed with DXP-NPs 1mg/kg (*eq.DXM*). Therefore, a higher dose of DSP would be needed to reach the same therapeutic efficacy as DXP-NPs 1mg/kg (*eq.DXM*) with potentially more severe associated side effects. Altogether, these results showed that DXP-NPs are safe after IV administration on CIA mice at a therapeutic dose of 1mg/kg (*eq.DXM*).

4 Conclusion

In this study, the lipophilic prodrug of dexamethasone, DXP, was successfully stabilized by the sole addition of DSPE-PEG_{2000} to yield nanoparticles as perfect candidates for RA treatment. For the first time, these highly loaded, stable, and stealth DXP-NPs demonstrated their clinical relevance in the CIA mouse model. Owing to their small size of 130nm and dense PEG coating, DXP-NPs could benefit

from the typical high vascular permeability of inflamed joints and diffuse passively to accumulate and be retained in the diseased sites as demonstrated by *in vivo* NIR fluorescence imaging. This accumulation in inflamed joints led to improvement of the joint inflammation and eventually disease remission. After three IV injections of DXP-NPs 1mg/kg (*eq.DXM*), the arthritis symptoms such as joint edema, swelling and ankylosis were significantly reduced compared to free hydrosoluble dexamethasone and to PBS injections. Moreover, this macroscopic evaluation was correlated with a significant reduction of histological signs of inflammation. Biologic and hematologic parameters were quantified to evaluate the potentially induced side effects of DXP-NPS at the efficient therapeutic dose of 1mg/kg (*eq.DXM*) and no adverse effects were detected for DXP-NPs. Considering the actual therapeutic scheme of RA patients, the developed DXP-NPs could be considered as a promising treatment for acute inflammation stage to prevent cartilage and bone erosion, in monotherapy or in combination with current 1st line treatment such as methotrexate.

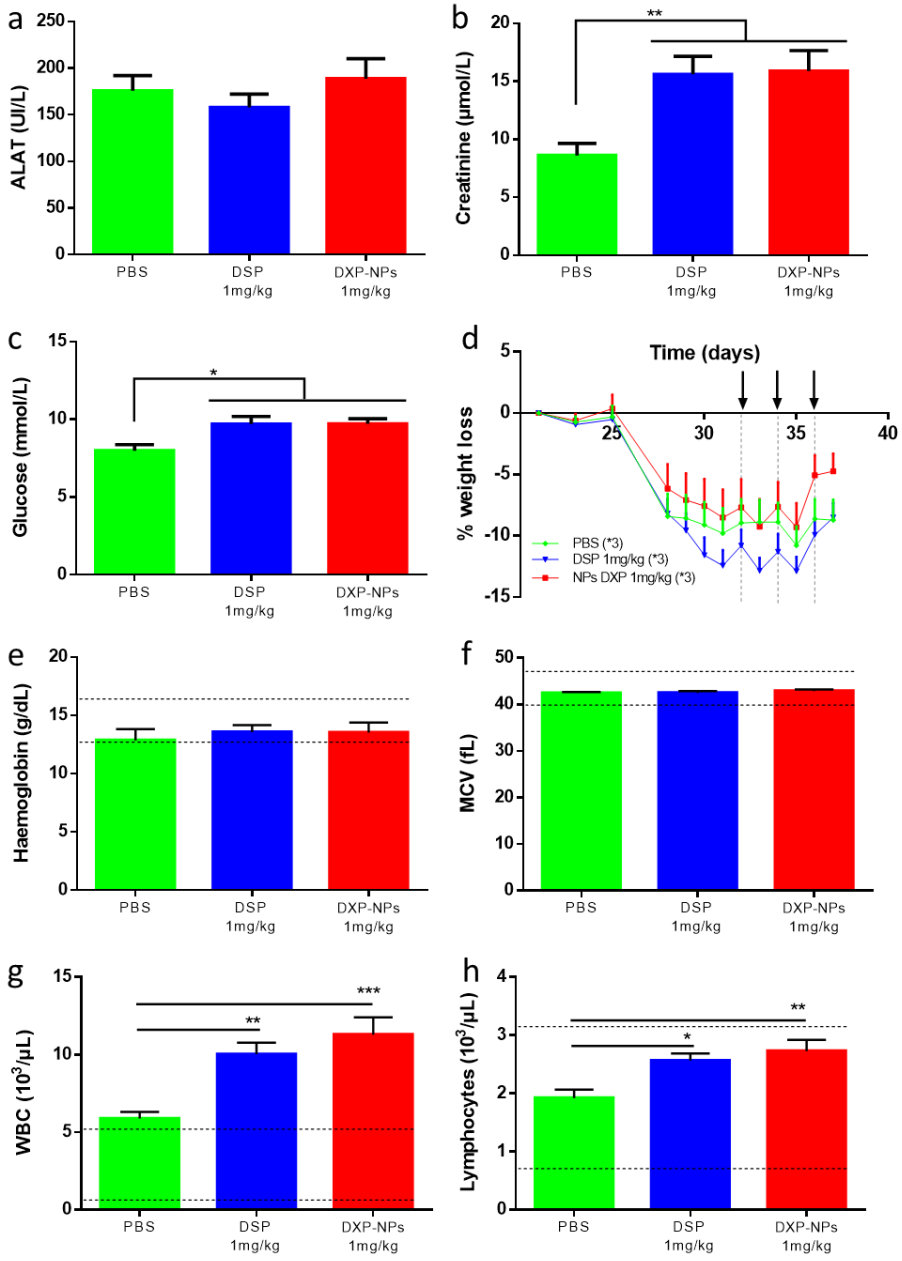

Fig. 6. DXP-NPs administration does not lead to adverse effects compared to DSP administration. Three groups of CIA mice (n=10) received PBS, or DSP 1mg/kg (eq.DXM) or DXP-NPs 1mg/kg (eq.DXM) on days 32, 34 and 36 after CIA induction. Mice were followed up to sacrifice on day 37, several biological parameters were analyzed. **a.** No difference between groups was detected for ALAT (alanine aminotransferase) plasmatic concentration. Plasmatic creatinin (**b**) and glucose (**c**) concentrations were similar for treatment groups (DSP and DXP-NPs) but presented a slight increase compared to PBS group. **d.** The weight of each animal was recorded from day 21 to day 37. No significant difference was observed although DXP-NPs treated mice lost less weight compared to PBS and DSP groups. **e-h.** Hematological parameters were analyzed on total blood, dotted lines on graphs represent standard values for healthy mice. No anemia was observed on any group of treatment or PBS with hemoglobin concentration values within the normal range (**e**) as well as for mean corpuscular volume (MCV) (**f**). CIA mice treated with PBS presented an increased white blood cell (WBC) count (**g**) compared to standard values. Leukocytosis was also observed for DSP and DXP-NPs group of treatments with a significant difference with PBS. **h.** The presence of lymphocytes slightly increased after DSP and DXP-NPs administration, but values were still consistent with standard ones.

Results are presented as mean ± SEM (n=10). Statistical analysis was performed with One-Way ANOVA followed by Tukey's post-test (*p<0.05, **p<0.01, ***p<0.001).

Conflict of interest

None.

Acknowledgments

M. L. PhD fellowship has been funded by Ministère de l'Enseignement Supérieur et de la Recherche. M. R. was supported by a fellowship from Campus France. The present work has benefited from the core facilities of Imagerie-Gif, (http://www.i2bc.paris-saclay.fr), member of IBiSA (http://www.ibisa.net), supported by "France-BioImaging" (ANR-10-INBS-04-01), and the Labex "Saclay Plant Science" (ANR-11-IDEX-0003-02) with the precious help of C. Boulogne and C. Gillet. Institut Galien Paris-Sud is a member of the Laboratory of Excellence LERMIT supported by a grant from ANR (ANR-10-LABX-33). M.E was supported by a Junior Team Leader starting grant from the LabEx LERMIT and an ANR @RAction starting grant (ANR-14-ACHN-0008).

References

[1] G.J. Tobón, P. Youinou, A. Saraux, The environment, geo-epidemiology, and autoimmune disease: Rheumatoid arthritis., Autoimmun. Rev. 9 (2010) A288-92. doi:10.1016/j.autrev.2009.11.019.

[2] Y. Alamanos, A.A. Drosos, Epidemiology of adult rheumatoid arthritis, Autoimmun. Rev. 4 (2005) 130–136. doi:10.1016/j.autrev.2004.09.002.

[3] R. Khurana, S.M. Berney, Clinical aspects of rheumatoid arthritis., Pathophysiology. 12 (2005) 153–65. doi:10.1016/j.pathophys.2005.07.009.

[4] C.C. Erhardt, P. a Mumford, P.J. Venables, R.N. Maini, Factors predicting a poor life prognosis in rheumatoid arthritis: an eight year prospective study., Ann. Rheum. Dis. 48 (1989) 7–13.

[5] D.L. Scott, F. Wolfe, T.W.J. Huizinga, Rheumatoid arthritis, Lancet. 376 (2010) 1094–1108. doi:10.1016/S0140-6736(10)60826-4.

[6] Z. Szekanecz, T. Besenyei, G. Paragh, A.E. Koch, Angiogenesis in rheumatoid arthritis., Autoimmunity. 42 (2009) 563–73.

[7] P.R. Colville-Nash, D.L. Scott, Angiogenesis and rheumatoid arthritis: pathogenic and therapeutic implications., Ann. Rheum. Dis. 51 (1992) 919–925. doi:10.1136/ard.51.7.919.

[8] E.W. a M. Paleolog, S. Young, A.C. Stark, R. V Mccloskey, M. Feldma, R.N. Main, Modulation of Angiogenic Vascular Endothelial Growth Factor By Tumor Necrosis Factor Ix and Interleukin-1 in Rheumatoid Arthritis, Arthritis Rheum. (1998) 1258–1265.

[9] J.F. Ferreira, A.A. Ahmed Mohamed, P. Emery, Glucocorticoids and Rheumatoid Arthritis,

Rheum. Dis. Clin. North Am. 42 (2016). doi:10.1016/j.rdc.2015.08.006.

[10] A.K. McDonough, J.R. Curtis, K.G. Saag, The epidemiology of glucocorticoid-associated adverse events., Curr. Opin. Rheumatol. 20 (2008) 131–137.

[11] K.G. Saag, R. Koehnke, J.R. Caldwell, R. Brasington, L.F. Burmeister, B. Zimmerman, J. a Kohler, D.E. Furst, Low dose long-term corticosteroid therapy in rheumatoid arthritis: an analysis of serious adverse events., Am. J. Med. 96 (1994) 115–23.

[12] N.C. Nicolaides, Z. Galata, T. Kino, G.P. Chrousos, E. Charmandari, The human glucocorticoid receptor: molecular basis of biologic function., Steroids. 75 (2010) 1–12. doi:10.1016/j.steroids.2009.09.002.

[13] S. Vandevyver, L. Dejager, C. Libert, On the trail of the glucocorticoid receptor: into the nucleus and back., Traffic. 13 (2012) 364–74. doi:10.1111/j.1600-0854.2011.01288.x.

[14] K.G. Saag, Low-dose corticosteroid therapy in rheumatoid arthritis: balancing the evidence., Am. J. Med. 103 (1997) 31S–39S.

[15] C.T.N. Pham, Nanotherapeutic approaches for the treatment of rheumatoid arthritis, Wiley Interdiscip. Rev. Nanomedicine Nanobiotechnology. 3 (2011) 607–619. doi:10.1002/wnan.157.

[16] S. Dolati, S. Sadreddini, D. Rostamzadeh, M. Ahmadi, F. Jadidi-Niaragh, M. Yousefi, Utilization of nanoparticle technology in rheumatoid arthritis treatment, Biomed. Pharmacother. 80 (2016) 30–41. doi:10.1016/j.biopha.2016.03.004.

[17] B. Ozbakir, B.J. Crielaard, J.M. Metselaar, G. Storm, T. Lammers, Liposomal corticosteroids for the treatment of inflammatory disorders and cancer, J. Control. Release. 190 (2014) 624–636. doi:10.1016/j.jconrel.2014.05.039.

[18] C. Gómez-Gaete, N. Tsapis, M. Besnard, A. Bochot, E. Fattal, Encapsulation of dexamethasone into biodegradable polymeric nanoparticles, Int. J. Pharm. 331 (2007) 153–159. doi:10.1016/j.ijpharm.2006.11.028.

[19] Y. Avnir, R. Ulmansky, V. Wasserman, S. Even-Chen, M. Broyer, Y. Barenholz, Y. Naparstek, Amphipathic weak acid glucocorticoid prodrugs remote-loaded into sterically stabilized nanoliposomes evaluated in arthritic rats and in a Beagle dog: a novel approach to treating autoimmune arthritis., Arthritis Rheum. 58 (2008) 119–29. doi:10.1002/art.23230.

[20] R. Anderson, A. Franch, M. Castell, F.J. Perez-Cano, R. Bräuer, D. Pohlers, M. Gajda, A.P. Siskos, T. Katsila, C. Tamvakopoulos, U. Rauchhaus, S. Panzner, R.W. Kinne, Liposomal encapsulation enhances and prolongs the anti-inflammatory effects of water-soluble dexamethasone phosphate in experimental adjuvant arthritis., Arthritis Res. Ther. 12 (2010) R147. doi:10.1186/ar3089.

[21] M. Teshima, S. Kawakami, K. Nishida, J. Nakamura, T. Sakaeda, H. Terazono, T. Kitahara, M.

Nakashima, H. Sasaki, Prednisolone retention in integrated liposomes by chemical approach and pharmaceutical approach, J. Control. Release. 97 (2004) 211–218. doi:10.1016/j.jconrel.2004.03.011.

[22] H. Benameur, G. De Gand, R. Brasseur, J.P. Van Vooren, F.J. Legros, Liposome-incorporated dexamethasone palmitate : Chemical and physical properties, Int. J. Pharm. 89 (1993) 157–167.

[23] S. Hong Kee, K. Hack Joo, K. Hyun Pyo, H.J. Lee, B. Si Myung, Liposomes with anti-inflammatory steroid prednisolone palmitate, Drug Dev. Ind. Pharm. 4 (1988) 765–777.

[24] L. Quan, Y. Zhang, B.J. Crielaard, A. Dusad, S.M. Lele, C.J.F. Rijcken, J.M. Metselaar, H. Kostková, T. Etrych, K. Ulbrich, F. Kiessling, T.R. Mikuls, W.E. Hennink, G. Storm, T. Lammers, D. Wang, Nanomedicines for inflammatory arthritis: Head-to-head comparison of glucocorticoid-containing polymers, micelles, and liposomes, ACS Nano. 8 (2014) 458–466. doi:10.1021/nn4048205.

[25] R. Wang, R. Xiao, Z. Zeng, L. Xu, J. Wang, Application of poly(ethylene glycol)-distearoylphosphatidylethanolamine (PEG-DSPE) block copolymers and their derivatives as nanomaterials in drug delivery, Int. J. Nanomedicine. 7 (2012) 4185–4198. doi:10.2147/IJN.S34489.

[26] M. Doi, T. Ishida, S. Sugio, T. Imagawa, M. Inoue, Physicochemical properties of dexamethasone palmitate, a high fatty acid ester of an anti-inflammatory drug: polymorphism and crystal structure., J. Pharm. Sci. 78 (1989) 417–22.

[27] Y. Mizushima, T. Hamano, K. Yokoyama, Tissue distribution and anti-inflammatory activity of corticosteroids incorporated in lipid emulsion., Ann. Rheum. Dis. 41 (1982) 263–267.

[28] J.-K. Kim, M.D. Howard, T.D. Dziubla, J.J. Rinehart, M. Jay, X. Lu, Uniformity of drug payload and its effect on stability of solid lipid nanoparticles containing an ester prodrug., ACS Nano. 5 (2011) 209–16. doi:10.1021/nn102357y.

[29] X. Lu, M.D. Howard, M. Mazik, J. Eldridge, J.J. Rinehart, M. Jay, M. Leggas, Nanoparticles containing anti-inflammatory agents as chemotherapy adjuvants: optimization and in vitro characterization., AAPS J. 10 (2008) 133–140. doi:10.1208/s12248-008-9013-z.

[30] N. Grabowski, H. Hillaireau, J. Vergnaud, N. Tsapis, M. Pallardy, S. Kerdine-Römer, E. Fattal, Surface coating mediates the toxicity of polymeric nanoparticles towards human-like macrophages, Int. J. Pharm. 482 (2015) 75–83. doi:10.1016/j.ijpharm.2014.11.042.

[31] D.D. Brand, K. a Latham, E.F. Rosloniec, Collagen-induced arthritis., Nat. Protoc. 2 (2007) 1269–75. doi:10.1038/nprot.2007.173.

[32] U. Rauchhaus, F.W. Schwaiger, S. Panzner, Separating therapeutic efficacy from glucocorticoid side-effects in rodent arthritis using novel, liposomal delivery of dexamethasone phosphate:

long-term suppression of arthritis facilitates interval treatment., Arthritis Res. Ther. 11 (2009) R190. doi:10.1186/ar2889.

[33] J.M. Metselaar, M.H.M. Wauben, J.P.A. Wagenaar-Hilbers, O.C. Boerman, G. Storm, Complete remission of experimental arthritis by joint targeting of glucocorticoids with long-circulating liposomes, Arthritis Rheum. 48 (2003) 2059–2066. doi:10.1002/art.11140.

[34] J. Lu, T. Kasama, K. Kobayashi, Y. Yoda, F. Shiozawa, M. Hanyuda, M. Negishi, H. Ide, M. Adachi, Vascular endothelial growth factor expression and regulation of murine collagen-induced arthritis., J. Immunol. 164 (2000) 5922–7. doi:10.4049/jimmunol.164.11.5922.

[35] Z. Szekanecz, A.E. Koch, Vascular involvement in rheumatic diseases: "vascular rheumatology"., Arthritis Res. Ther. 10 (2008) 224. doi:10.1186/ar2515.

[36] T. Garrood, C. Pitzalis, Targeting the inflamed synovium: the quest for specificity., Arthritis Rheum. 54 (2006) 1055–60. doi:10.1002/art.21720.

[37] W. Hofkens, R. Schelbergen, G. Storm, W.B. van den Berg, P.L. van Lent, Liposomal Targeting of Prednisolone Phosphate to Synovial Lining Macrophages during Experimental Arthritis Inhibits M1 Activation but Does Not Favor M2 Differentiation, PLoS One. 8 (2013) e54016. doi:10.1371/journal.pone.0054016.

[38] J.M. Metselaar, W.B. van den Berg, A.E.M. Holthuysen, M.H.M. Wauben, G. Storm, P.L.E.M. van Lent, Liposomal targeting of glucocorticoids to synovial lining cells strongly increases therapeutic benefit in collagen type II arthritis., Ann. Rheum. Dis. 63 (2004) 348–53. doi:10.1136/ard.2003.009944.

[39] Y. Shoenfeld, Y. Gurewich, L. a Gallant, J. Pinkhas, Prednisone-induced leukocytosis, Am. J. Med. 71 (1981) 773–8. doi:10.1016/0002-9343(81)90363-6.

[40] M. Nakagawa, T. Terashima, Y. D'yachkova, G.P. Bondy, J.C. Hogg, S.F. Van Eeden, B. Marrow, Glucocorticoid-Induced Granulocytosis, Circulation. 98 (1998) 2307–2313.

[41] W. Grassi, R. De Angelis, G. Lamanna, C. Cervini, The clinical features of rheumatoid arthritis., Eur. J. Radiol. 27 Suppl 1 (1998) S18-24.